To be published in Astronomy Letters, Vol. 28, No. 12, 2002, pp. 811-820

Translated from Pis'ma v Astronomicheskij Zhurnal, Vol. 28, No. 12, 2002, pp. 902-912

Quasi-Periodic X-ray Oscillations in the Source Sco X-1

Sergey Kuznetsov*

Space Research Institute, Profsoyuznaya 84/32, Moscow, 117997 Russia

Received: July 5, 2002

The RXTE observations of Scorpius X-1 in 1996–1999 are presented. The properties of its quasi-periodic X-ray oscillations are studied in detail. The results obtained are used for analysis in terms of the transition-layer model (TLM) and the relativistic-precession model (RPM) for a slowly rotating neutron star. Theoretical predictions of the two models are compared and their self-consistency is verified. The tilt of the magnetosphere to the accretion-disk plane, the neutron-star mass, and its angular momentum are determined in the model frameworks.

Key words: accretion, neutron stars, Scorpius X-1, X-ray sources, low-mass binary X-ray sources, quasi-periodic oscillations.

1. Introduction

Scorpius X-1 is a low-mass X-ray binary with an accreting neutron star and one of the brightest X-ray sources. Its spectral properties suggest that Scorpius X-1 belongs to the class of Z-type sources (Hasinger and van der Klis 1989), whose characteristic feature is a Z-shaped track in the color–color diagram. In this interpretation, the spectral properties are presented in the hard–soft color indices, each of which is defined as the harder-to-softer flux ratio in the corresponding energy band. The Z-shaped track is commonly divided into three parts called branches: the horizontal (HB, the upper part of the diagram), normal (NB, the intermediate part), and flaring (FB, the lower part) branches. The position on the Z track is generally believed to be associated with the rate of accretion in the direction from HB to FB. Six sources are currently known to exhibit Z tracks in the color–color diagram: Scorpius X-1, Cygnus X-2, GX 17+2, GX 5-1, GX 340+0, and GX 349+2.

The power-density spectra (Fourier transforms of the flux) of Z-type sources exhibit low-frequency (5–100 Hz) X-ray quasi-periodic oscillation (QPO) peaks. The names of the QPOs correspond to

*Email: sik@hea.iki.rssi.ru

the branch with which their origin is identified: horizontal- (HBO), normal- (NBO), and flaring-branch (FBO) oscillations. HBOs (15–100 Hz) can also be detected in the NB spectral state. However, as one recedes from HB, the statistical significance of the QPO peaks decreases and they become undetectable. When moving along the Z track (from HB to FB) in its NB–FB segment, a QPO peak detectable in the range 5–20 HZ (NBO/FBO) emerges in the power-density spectra. For all the currently known Z-type sources, QPOs were also found in the range 200–1100 kHz (van der Klis 2000). Two kHz QPO peaks (ν_1 and ν_2 are the lower and upper peaks, respectively) can be simultaneously observed with a frequency difference of $\sim$ 200–400 Hz. For a series of successive observations (i.e., on short time scales from several hours to several days), an increase in the flux is accompanied by an increase in the frequencies of the two peaks, but their difference ($\Delta\nu = \nu_2 - \nu_1$) is not conserved (van der Klis et al. 1997).

The observations of Scorpius X-1 revealed all the QPO types characteristic of the low-frequency ($<$ 100 Hz) range in the power-density spectrum. At high frequencies, two kHz QPO peaks ($\nu_1 and \nu_2$) were found in the RXTE/PCA data [first detected by van der Klis et al. (1996)]. Here, we study the QPO properties in detail. Our results are used for analysis in terms of the transition-layer model (TLM) and the relativistic-precession model (RPM). We compare theoretical predictions of the two models and verify their self-consistency. The X-ray flux variability of the source at low frequencies (0.1–128 Hz) is investigated by taking into account the power-law behavior of the power-density spectrum at frequencies above and below the break frequency.

2. DATA AND OBSERVATIONS

For our time analysis, we used data from the PCA (Proportional Counter Array) instrument (Jahoda et al. 1996) onboard the RXTE observatory (Bradt et al. 1993) retrieved from the Goddard Space Flight Center Electronic Archive.

The source Scorpius X-1 was observed by the RXTE observatory during eleven series of pointing observations (10056, 10057, 10059, 10061, 20053, 20426, 30035, 30036, 30406, 40020, 40706): in February and May 1996, in March, April, and August 1997, in January, February, and from May until July 1998, and in January and July 1999. The observations of Scorpius X-1 over this period correspond to three different observational epochs of RXTE/PCA (1, 3, and 4 in the adopted classification), for which the boundaries of the PCA energy channels were changed.

To construct the power-density spectra, we used observational data with a resolution of $\sim$122 or $\sim$ 244 μm (2^{-13}, 2^{-12} s) from the zeroth to 87th or 249th PCA energy channels. These ranges (0–87 and 0–249) correspond to a detectable photon flux $\sim 1.5 - 23.5$, $\sim 1.9 - 32.3$, and $\sim 2.0 - 38$ keV for epochs 1, 3, and 4, respectively, or extend to $\sim$ 60 keV if the entire accessible PCA energy range (channels 0–249) was used.

Of all the observations, we used only those during which the angle between the source direction and the Earth's horizon was more than 10°. During the observations of Scorpius X-1, all five

proportional counters were not always switched on to record events. If the operating condition of one of the counters changed during a continuous observation (whose duration did not exceed the duration of one orbit and was, on average, $3 - 3.5 \times 10^3$ s), then the time interval during which the total count rate changed abruptly was excluded from our analysis.

To analyze the variability of Scorpius X-1, we constructed its power-density spectra (van der Klis 1989) in the frequency range 0.03125–2048 Hz (see Fig. 1). The properties of the low- and high-frequency flux variability were investigated in the bands 0.1–256 and 256–2048 Hz, respectively. No correction was made for the background radiation and dead time.

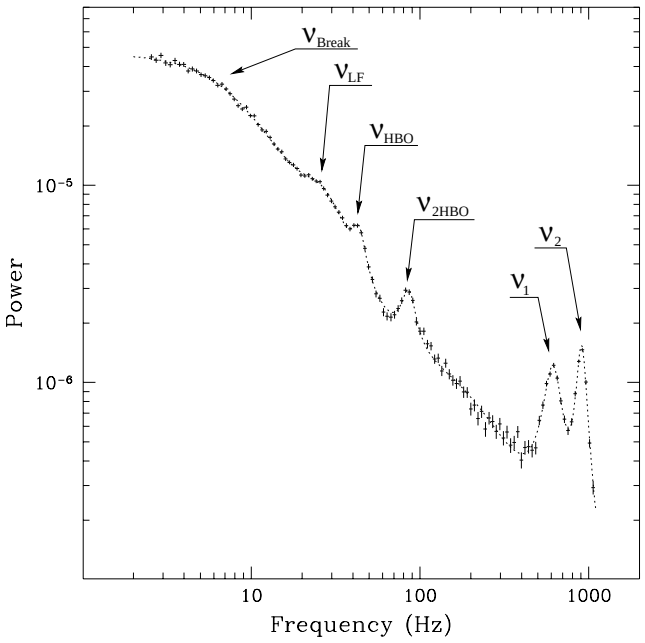

Fig. 1. The power-density spectrum for the Z-type source Scorpius X-1. The data were averaged over four consecutive observing intervals from 05 : 04 : 13 UTC on May 25, 1996. The total observing time is $\sim 10^4$ s [see a similar power-density spectrum in Titarchuk et al. (1999)]. The X-ray QPO peaks are shown: HBOs (ν_{HBO}) and their second harmonic (ν_{2HBO}) and the kHz QPO peaks (ν_1 and ν_2). The break frequency is denoted by ν_{Break}. A model fit to the data (for more details, see the text) is indicated by the dotted line. Broadband noise was detected at a statistically significant level in the average power-density spectrum at low frequencies (ν_{LF}).

We analyzed individual observations with a duration up to $\sim 3.5 \times 10^3$ s. Fitting the power-density spectra by a constant and by a power law at frequencies below and above the break frequency did not yield acceptable results (according to the χ^2 test). The main reason was the absence of a sharp break and the resulting uncertainty in its measurement. The model in which at frequencies much higher ($\nu/\nu_{break} \gg 1$) and much lower ($\nu/\nu_{break} \ll 1$) than the break, each part of the spectrum could be fitted by its own power law and the transition between them was not jumplike (previously, this model was successfully used for a time analysis of the Z-type source Cygnus X-2; see, e.g., Kuznetsov 2001), proved to be more suitable:

$$P(\nu) = A\nu^{-\alpha}[1 + (\nu/\nu_{\rm break})^{\beta}]^{-1}. \quad (1)$$

The power-density spectra (see Fig. 1) were fitted by this model in the 0.1–128-Hz band with the additional introduction of one or two Lorenz lines to allow for the QPO peaks and their harmonics.

To take into account the PCA dead-time effect, which causes the overall level to be shifted to the negative region [because of this effect, the Poissonian noise level subtracted from all spectra differed from 2.0, in units of the Leahy normalization; see van der Klis (1989) and Vikhlinin et al. (1994) for more details], we added a constant to the general model.

In searching for the kHz (in the range $\sim 500 - 1200$ Hz) QPO peaks ν_1 and ν_2, we analyzed the power-density spectra at high frequencies. A constant with the addition of one or two Lorenz lines was used as the model. Individual observations in which the detection confidence level of kHz QPO peaks exceeded 3σ were used for the subsequent analysis.

Our analysis of the low-frequency flux variability in Scorpius X-1 revealed QPOs at a high confidence level in all the individual observations that corresponded to the HB or NB spectral states. Note that the HBO frequency is one of the main frequencies in most models, including the TLM and RPM. The two models (see below) unequivocally establish the correspondence between the three QPO peaks: the HBOs, lower, and upper kHz QPOs.

To obtain the most accurate model parameters (the angle δ for the TLM and the neutron-star mass M_{NS} and angular momentum a for the RPM), which are invariants in each of the theories under consideration, it was necessary to calculate the three simultaneously observed main QPO frequencies (i.e., ν_{HBO}, ν_1, ν_2; see Fig. 1) as accurately as possible. Therefore, of all the preselected data in which both kHz QPO peaks (ν_1 and ν_2) were found, we used only those in which the main HBO peak (ν_{HBO}) and its second harmonic (ν_{2HBO}) were detected at a confidence level above 4σ. In such observations, the two kHz QPO peaks were also reliably detected.

3. LOW-FREQUENCY X-RAY FLUX VARIABILITY

3.1. The Power of the HBO peaks

In Fig. 2, rms is plotted against HBO frequency. The flux variability (i.e., rms^2) at the peak corresponds to the integral of the Lorenz line that fits best the QPO peak in the power-density spectrum. For the Z-type sources, to which Scorpius X-1 belongs, an increase in HBO frequency is accompanied by a decrease in rms (see, e.g., van der Klis 2000). As a result, the detection confidence level of HBO peaks is lower at high frequencies ($\sim 50 - 60$ Hz). Figure 2 shows the range of HBO frequencies found for Scorpius X-1. During all observations, the deviation from the mean $\nu_{HBO} \approx 43.5$ Hz did not exceed ~ 5 Hz (i.e., it changed by no more than 10% during all observations).

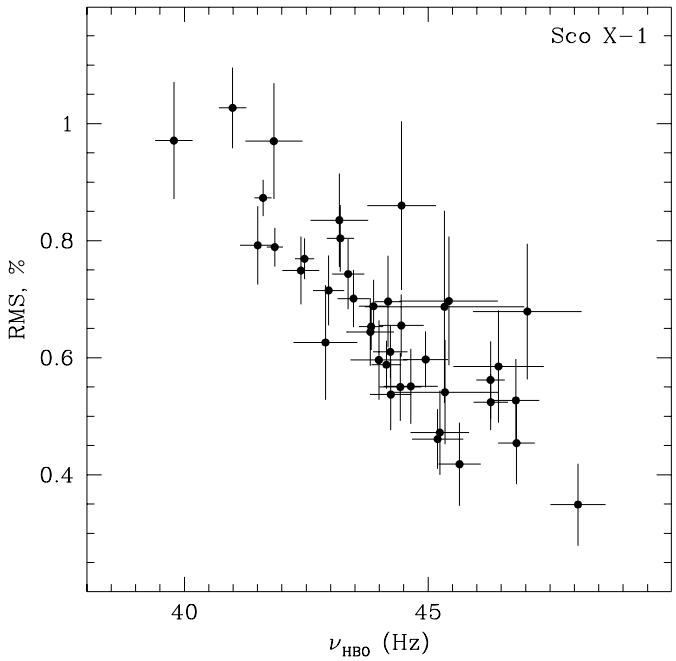

Fig. 2. The rms of the QPO peaks versus HBO frequency. Individual observations are presented. As rms decreases, the detection confidence level of the QPO peaks falls, reaching $\sim 4\sigma$ for rms in the range $\sim 0.4 - 0.5\%$.

3.2. Horizontal-Branch Oscillations and Their Harmonics

In Scorpius X-1, quasi-periodic HBO peaks were found at low frequencies (< 100 Hz). Together with the oscillations at the main frequency ν_{HBO}, we also found QPO peaks at frequencies close to the multiple ones. Note that the detection confidence level of HBO peaks decreases with frequency (see Fig. 2). That is why no multiple peaks were found (at a confidence level $> 4\sigma$) for which $\nu_{HBO} > 48$ Hz (the corresponding oscillation frequency of the second harmonic is $\nu_{2HBO} > 96$ Hz).

The frequency ratio $r_{2/1} = \nu_{HBO}/\nu_{2HBO}$ of the multiple HBO harmonics is shown in Fig. 3. We clearly see that $r_{2/1}$ differs from 2.0: only a third of the 39 data points are above 2.0 (the dotted line in Fig. 3). Fitting by a constant yields $r_{2/1} = 1.965 \pm 0.004$, $\chi^2_{red} = 3.45$ (in what follows, $\chi^2_{red} = \chi^2/d.o.f$ is the reduced χ^2 value per degree of freedom), while fitting by a constant with a break yields $r_{2/1} = 1.976 \pm 0.004$, $\chi^2_{red} = 1.05$ (and $r_{2/1} = -0.05 \times (\nu_{HBO} - 45.31)$ in the range of a linear dependence). When the scatter of data points exceeds the stochastic scatter and when the χ^2_{red} value is much larger than unity (as in the case of a constant fit), it should be assumed that the uncertainty could be produced by stochastic processes rather than by the statistics alone. We can then ignore the measurement error and determine the mean $\bar{r}_{2/1} = \frac{1}{N}\sum r_{2/1}$ and the rms deviation from it $\sigma = \sqrt{\frac{\sum(r_{2/1}-\bar{r}_{2/1})^2}{(N-1)}}$. In this case, we obtained the following ratio of the second and first harmonics: $\bar{r}_{2/1} = 1.973$, $\sigma = 0.050$. Under such an assumption, the harmonic ratio is compatible with 2.0, within the error limits.

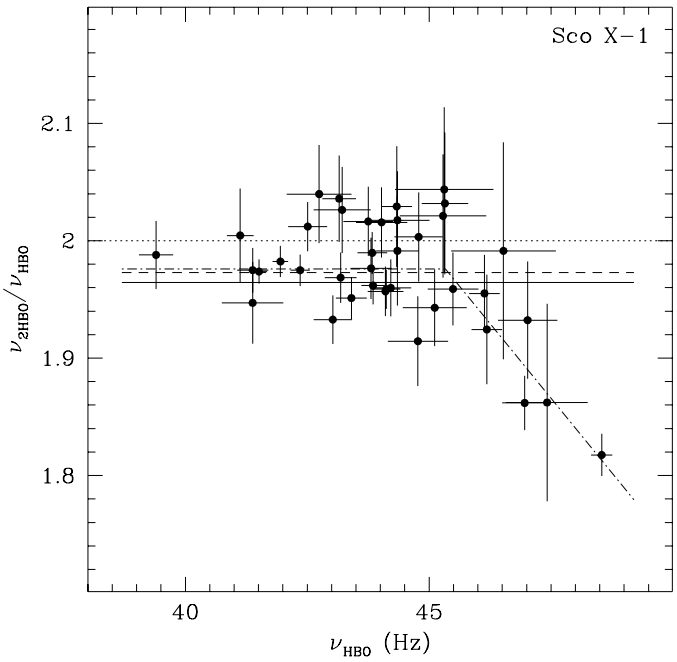

Fig. 3. The ratio of multiple HBO harmonics versus frequency ν_{HBO}. The solid, dash–dotted, dashed, and dotted lines represent, respectively, a constant fit to the data with statistical errors (minimization according to the χ^2 test), a constant fit with a break, the mean of individual observations (without errors), and the assumed harmonic ratio 2.0.

Let us consider in more detail the case where the scatter of $r_{2/1}$ values about the mean is determined by the statistics alone and is incompatible with 2.0, within the error limits. Resonances in nonlinear oscillatory systems can emerge at frequencies at which an external periodic force acts on the oscillator. This requires that its frequency γ satisfy the condition

$$\gamma = \omega_0 \frac{p}{q}, \tag{2}$$

where p and q are integers and ω_0 is the cyclic frequency of free system oscillations.

The power of the main peak must be maximal among all of the harmonics, because the intensity of resonance phenomena rapidly decreases with increasing p and q (Landau and Lifshitz 1965). In addition, if the frequency of the periodic external force γ differs from ω_0 by a small value ε (in the simplest case, $p = 1$ and $q = 1$), then in nonlinear oscillations, this can lead to a displacement of the rms maximum from the oscillator resonance frequency (Landau and Lifshitz 1965). In Scorpius X-1, the largest rms among all the HBO harmonics corresponds to the frequency ν_{HBO} (see Fig. 2). We assume from the outset that the latter (and this assumption proved to be valid) was the fundamental harmonic and the deviation of the frequency ratio of the second and first harmonics from 2.0 is admitted in the forced oscillations of a nonlinear oscillator under the action of a periodic force.

Note that in this case, the frequency of the observed low-frequency oscillation peak is $\nu_{HBO} \neq \omega_0/2\pi$. This is particularly important in comparing the self-consistency of the theoretical models under consideration, which interpret the emergence of QPOs (to be more precise, the following

three QPOs: ν_{HBO}, ν_1, and ν_2) in binary systems with neutron stars.

If the deviation of the ratio of the multiple HBO harmonics $\nu_{2/1}$ from 2.0 is assumed to be attributable to forced nonlinear oscillations, then the observed ν_{HBO} must be close but not exactly equal to $\omega_0/2\pi$, the assumed frequencies of free oscillations of the oscillator. Note that $\omega_0/2\pi$ rather than ν_{HBO} corresponds to the low-frequency QPOs in the models considered below.

For this reason, for our analysis in terms of each of the models considered below, we use two values for the low-frequency QPOs: ν_{HBO} and $\bar{\nu}_{HBO}$. These values are the fundamental HBO harmonic and the mean between half the frequency of the second harmonic ν_{2HBO} and the fundamental harmonic ν_{HBO}. For the latter case, from all the observations, we chose those in which the confidence level of each HBO peak was higher than 4σ.

4. THEORETICAL MODELS

For our analysis in terms of the two models in question, we used the average spectra and the main frequencies: ν_{HBO} (as well as $\bar{\nu}_{HBO} = 1/2(\nu_{HBO} + 1/2\nu_{2HBO})$, the mean between the fundamental harmonic and half the second harmonic), ν_1, ν_2. The following approximate asymptotic relations between the frequencies are known from the observations of low-mass X-ray binaries (Stella et al. 1999): (1) $\Delta\nu = \nu_2 - \nu_1 \propto \nu_2^2$; and (2) $\nu_{HBO} \propto \nu_1$. These observed features are consistent with each of the theories under consideration.

4.1. The Transition-Layer Model (TLM)

We consider the motion of a clump of matter, the QPO source on the accretion-disk surface, in a Keplerian orbit around a neutron star (NS) in terms of this model. The magnetospheric axis is assumed to be not aligned with the normal to the disk surface but makes an angle δ. After multiple passages through a slightly tilted magnetosphere, the clump comes under the effect of Coriolis forces. These forces cause the main Keplerian oscillation frequency ν_K to split up into two oscillation modes: radial (ν_h) and perpendicular to the disk plane (ν_L). The two modes are the solution of the equation for the rotation of a body in a noninertial frame of reference [see Osherovich and Titarchuk (1999) for more details on its derivation and solution]. In this model, the lower and upper kHz QPO peaks correspond to the Keplerian ($\nu_K \equiv \nu_1$) and hybrid ($\nu_h \equiv \nu_2$) frequencies, respectively. The relation between the kHz QPO peaks is given by

$$\nu_h = [\nu_K^2 + (\Omega/\pi)^2]^{1/2}, \tag{3}$$

where Ω is the angular velocity of the magnetosphere. The oscillation mode perpendicular to the disk surface is defined as

$$\nu_L = (\Omega/\pi)(\nu_K/\nu_h)\sin\delta. \tag{4}$$

Since all three characteristic frequencies ν_L, ν_K, and ν_h are known from observations, the sought-for angle δ can be calculated by using (4):

$$\delta = \arcsin[(\nu_h^2 - \nu_K^2)^{-1/2}(\nu_L\nu_h/\nu_K)]. \quad (5)$$

To a first approximation, the angular velocity of the magnetosphere Ω is constant. A more accurate equation that describes the dependence of Ω on radius can be derived in the multipole magnetic-field approximation (see Osherovich et al. 1984). Assuming the contribution of the quadrupole component to the magnetic-field strength in the equatorial plane to be negligible and taking into account the dipole and octupole components, the final equation for the angular velocity can be represented as (Osherivich and Titarchuk 1999)

$$\Omega/2\pi = C_0 + C_1\nu_K^{4/3} + C_2\nu_K^{8/3} + C_3\nu_K^4, \quad (6)$$

with $C_2 = -2(C_1C_3)^{1/2}$.

To reconstruct the magnetospheric profile for Scorpius X-1, according to Eq. (3), it will suffice to have data only for the high-frequency range of the flux variability, i.e., ν_1 and ν_2. Therefore, we used all the data in which kHZ QPO peaks were found by removing the additional condition that the main HBO peak ν_{HBO} and its second harmonic ν_{2HBO} should be detected in the power-density spectrum at low frequencies at a confidence level above 4σ.

The angular velocity is plotted against Keplerian frequency in Fig. 4. Using (6), we managed to obtain the magnetospheric profile suggested by the model under consideration with the following parameters: $C_0 = 354$ Hz, $C_1 = -3.54 \times 10^{-2}$ Hz$^{-1/3}$, $C_2 = 9.99 \times 10^{-6}$ Hz$^{-5/3}$, and $C_3 = -7.21 \times 10^{-10}$ Hz^{-3}. In fitting the data, we assumed C_2 to be a free parameter, whereas in the model, $C_2 = -2(C_1C_3)^{1/2} = 1.01\times10^{-5}$. The similar values of C_2 determined by two independent methods are a weighty argument for the approximation used for the magnetospheric profile.

Using (5), we obtained δ for each triplet of frequencies: ν_{HBO}, ν_1, and ν_2. In Fig. 5 the HBO frequency ν_{HBO} is plotted against the angle δ between the normal to the disk surface and the magnetospheric axis. Among all three frequencies used in calculating δ, the strongest correlation is observed between δ and ν_{HBO}. For this reason, the dependence of δ on low-frequency QPOs is analyzed in the model under consideration (below, we show that this is also true for the relativistic precession model), because the model invariants must be conserved, irrespective of the measured QPO frequency range.

Table 1 gives data on the constant fit to δ in two cases: when $\nu_L = \nu_{HBO}$ (see Fig. 5) and $\nu_L = \bar{\nu}_{HBO} = 1/2(\nu_{HBO} + 1/2\nu_{2HBO})$ (see Fig. 6), i.e., with the inclusion of the second HBO harmonic. The χ^2_{red} value is given in each case. The mean angle $\bar{\delta}$ and its rms deviation σ_D are also given in Table. 1.

To reduce the possible stochastic scatter of data points (which probably dominates over the statistical scatter), we performed averaging depending on the HBO frequency. The upper panels in Figs. 5 and 6 show the data obtained in this way. Whereas the data in Fig. 5 reveal a clear correlation

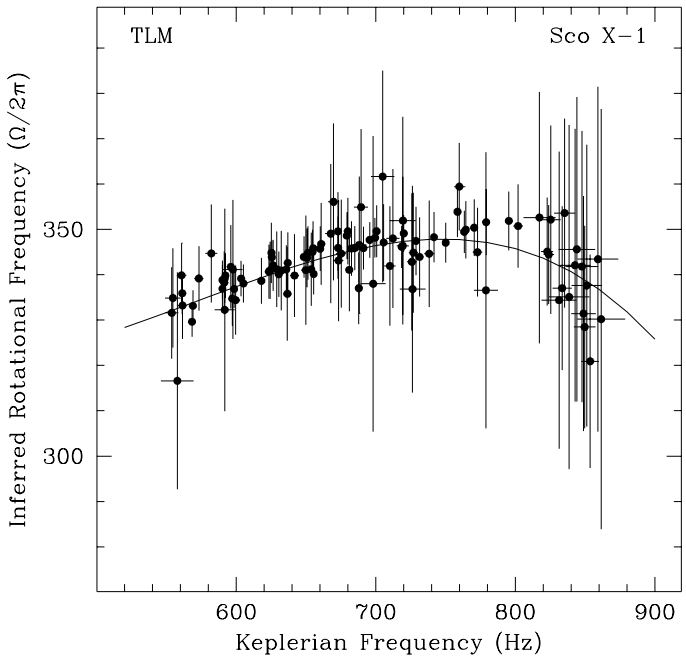

Fig. 4. The assumed angular velocity of the magnetosphere in the TLM, in units of $\Omega/2\pi$, versus Keplerian frequency ($\nu_K = \nu_1$).

between δ and ν_{HBO}, the data points in Fig. 6 virtually lie on the same line. If a larger number of points in each bin were averaged (in our case, we combined them by five), then δ (see Fig. 6, where δ is plotted against $\bar{\nu}_{HBO}$) would be even more compatible with a constant, according to the χ^2 test.

Let us compare the rms deviation between the HBO harmonic ratio $r_{2/1}$ determined above and δ (see Table 1). It turns out that $\sigma_{r_{2/1}} \approx 2.5\%$, while $\sigma_\delta \approx 2.0\%$. Since, according to (5), $\delta \propto \nu_{HBO}$ at small angles and since ν_{HBO} increasingly deviates from $\omega/2\pi$ to larger values with decreasing $r_{2/1}$, the correlation for δ (clearly seen only in Fig. 5) can result from the emergence of nonlinear oscillations considered in the previous sections.

4.2. The Relativistic Precession Model (RPM)

The high-velocity motion of matter in a strong gravitational field can generate oscillations attributable to general-relativity effects. The RPM (see, e.g., Morsink et al. 1999) considers the motion of a point mass around a gravitating center. If a particle moves in an orbit that does not lie exactly in the equatorial plane of a compact object but is inclined at an infinitesimal angle, then the particle orbit will precess.

For a nonrotating gravitating center (i.e., in the Schwarzschild approximation), the expression for

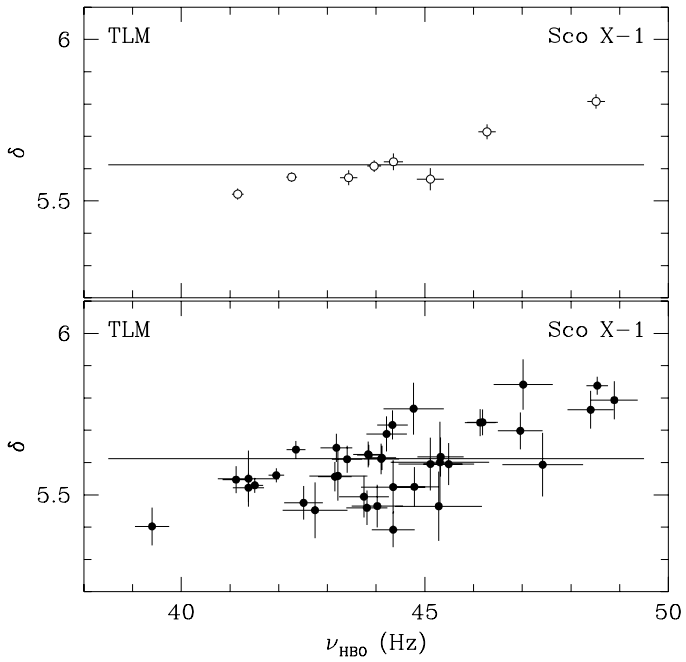

Fig. 5. The angle between the magnetospheric axis and the normal to the disk surface versus HBO frequency $\nu_{HBO} \equiv \nu_L$. A constant fit is indicated by the solid line. The lower panel shows individual observations of Scorpius X-1 with a duration up to $\sim$ 3.5 ks. The upper panel shows the same observations as in the lower panel averaged over five points according to the frequency ν_{HBO}.

the particle angular velocity matches the classical formula for Keplerian motion. However, for a NS or a black hole with an intrinsic angular momentum, the azimuthal frequency can be expressed (Bardeen et al. 1972; Stella et al. 1999) in a system of units with $G = 1$ and $c = 1$ as

$$\nu_\phi = \sqrt{\frac{M}{r^3}} \left[2\pi \left(1 + a\sqrt{\frac{M}{r^3}} \right) \right]^{-1}. \tag{7}$$

Below, we consider only the case where the compact object and the test particle corotate: $\nu_\phi > 0, a > 0$ (a is the relative angular momentum). The epicyclic frequency ν_r together with the azimuthal frequency ν_ϕ determine the orbital periastron rotation, $\nu_{per} \equiv \nu_\phi - \nu_r$, while the frequency in a direction perpendicular to the disk plane ν_θ determines the nodal precession, $\nu_{nod} \equiv |\nu_\phi - \nu_\theta|$. The corresponding equations were derived by Okazaki et al. (1987) and Kato (1990):

$$\nu_r = \nu_\phi \sqrt{1 - 6\frac{M}{r} + 8a\sqrt{\frac{M}{r^3}} - 3\frac{a^2}{r^2}}, \tag{8}$$

$$\nu_\theta = \nu_\phi \sqrt{1 - 4a\sqrt{\frac{M}{r^3}} + 3\frac{a^2}{r^2}}. \tag{9}$$

In contrast to the TLM, the Keplerian rotation frequency in the RPM corresponds to the upper QPO peak, $\nu_2 = \nu_\phi$, while the observed periastron precession frequency corresponds to the lower

Tabl. 1. The angle between the normal to the disk surface and the magnetospheric axis for various HBO values.

Parameter	$\nu_L = \nu_{HBO}$	$\nu_L = \bar{\nu}^a_{HBO}$
δ	5.612 ± 0.007	5.545 ± 0.006
$\chi^2_{\rm red}$	5.53	2.94
$\bar{\delta}^b$	5.600 ± 0.114	5.555 ± 0.086
N, bin	39	39

[a] $\bar{\nu}_{HBO} = 1/2(\nu_{HBO} + 1/2\nu_{2HBO})$.
[b] The quantity $\bar{\delta}$ is the mean of all δ with the error σ_D equal to the standard deviation.

QPO peak, $\nu_1 = \nu_{per} \equiv \nu_\phi - \nu_r$. In the Kerr approximation, $\nu_\phi \neq \nu_\theta$ (for the Schwarzschild case with $a = 0$, the frequencies are equal: $\nu_\phi = \nu_\theta$), the HBOs are identified with nodal precession: $\nu_{nod} \equiv |\nu_\phi - \nu_\theta|$. Some authors (e.g., Stella et al. 1999) believe that ν_{HBO} is an even harmonic of ν_{nod}. In contrast to $\nu_{HBO} = \nu_{nod}$, this relation causes the mass of the compact source in Eqs. (7)–(9) required by the RPM to decrease.

In the RPM approximation under consideration, the NS mass and relative angular momentum are invariants and do not depend on Keplerian frequency. Thus, we can determine M_{NS} and a from Eqs. (7)–(9) using the three observed main frequencies: ν_{HBO}, ν_1, and ν_2.

As in the section devoted to the TLM, here, the invariant (more specifically, the NS mass M_{NS} suggested by the model) was also determined in two cases: $\nu_{nod} = \nu_{HBO}$ and $\nu_{nod} = \bar{\nu}_{HBO} = 1/2(\nu_{HBO} + 1/2\nu_{2HBO})$ (i.e., with the inclusion of the second HBO harmonic). Since the derived M_{NS} proved to be most dependent (as in the TLM) on low-frequency HBOs, Figs. 7 and 8 show M_{NS} as a function of ν_{HBO}.

Tabl. 2. The NS mass and its relative angular momentum for various HBO values.

Parameter	$\nu_{nod} = \nu_{HBO}{}^a$	$\nu_{nod} = \bar{\nu}_{HBO}$	$2\nu_{nod} = \nu_{HBO}$	$2\nu_{nod} = \bar{\nu}_{HBO}{}^a$
$M_{NS}, M_\odot$	2.680 ± 0.002	2.675 ± 0.002	2.339 ± 0.002	2.338 ± 0.002
χ^2_{red}	14.3	16.3	16.4	17.5
$\bar{M}^b_{NS}, M_\odot$	2.677 ± 0.050	2.674 ± 0.053	2.341 ± 0.045	2.341 ± 0.045
a^c,	1367 ± 2	1358 ± 2	663 ± 1	658 ± 1
χ^2_{red}	8.2	13.7	8.2	13.6
N, bin	39	39	39	39

[a] $\bar{\nu}_{HBO} = 1/2(\nu_{HBO} + 1/2\nu_{2HBO})$.
[b] $\bar{M}_{NS}$ corresponds to the mean of all M_{NS} with the error equal to the standard deviation σ_D.
[c] $a = J/(c \times M_{NS})$.

Table 2 gives a constant fit to the data (shown in Figs. 7 and. 8). We clearly see a large χ^2_{red} value

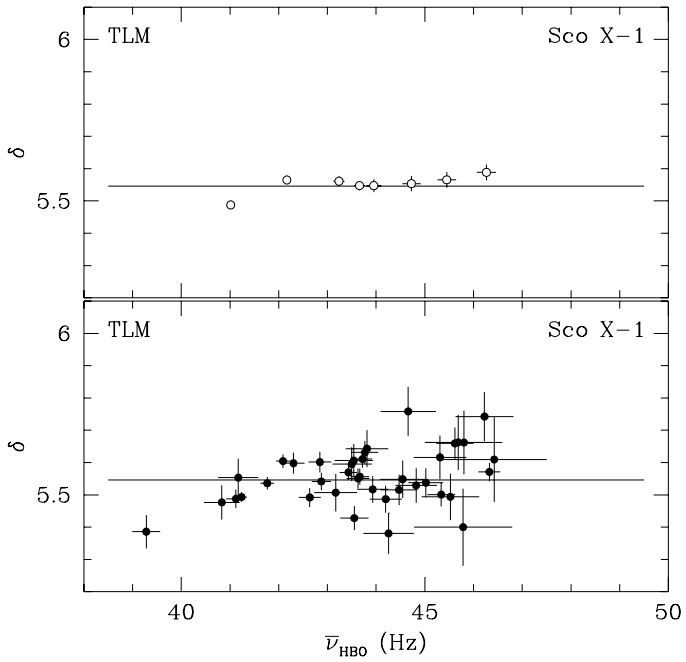

Fig. 6. The angle between the magnetospheric axis and the normal to the disk surface versus HBO frequency $\bar{\nu}_{HBO} \equiv \nu_L = 1/2(\nu_{HBO} + 1/2\nu_{2HBO})$. A constant fit is indicated by the solid line. The lower panel shows individual observations of Scorpius X-1 with a duration up to ~ 3.5 ks. The upper panel shows the same observations as in the lower panel averaged over five points according to the frequency ν_{HBO}.

for each ν_{nod}: compared to Table. 1, which gives a fit to δ (in the TLM), the corresponding χ^2_{red} values are larger by a factor of $\sim 3-6$. Nevertheless, the rms deviation $\sigma_{M_{NS}}$ is also $\approx 2.0\%$, as is σ_δ in the TLM. In contrast to Fig. 4, in which δ is plotted against $\bar{\nu}_{HBO}$ and is essentially compatible with a constant, we clearly see a linear correlation of M_{NS} with $\bar{\nu}_{HBO}$ in Fig. 8: as $\bar{\nu}_{HBO}$ increases from ~ 39.5 Hz to ~ 46.5 Hz, the required M_{NS} decreases from $\sim 2.8 M_\odot$ to $\sim 2.6 M_\odot$.

The relativistic precession model makes it possible to estimate the compact-source mass and to determine the Keplerian orbital radius. For comparison, Fig. 9 shows the mass–radius relations for various equations of state for neutron stars taken from Miller et al. (1998).

4.3. Comparison between the Assumed Invariants of the Models under Consideration

To check whether the two models are self-consistent and to determine whether the derived invariants δ and M_{NS} correlate with the HBO frequency (see Fig. 5–9), we used Spearman's nonparametric correlation test. The coefficient r_s equal to unity in magnitude points to a total correlation between the two quantities. In each case under consideration, we give the probability (prob) that the correlation found is the result of statistical fluctuations. This test is also convenient in the case where it is necessary to establish which of the several correlations under consideration is strongest. Our estimates are given in Tables 3 and 4. Note that the data in Table 4 correspond to the case where the statistical scatter was slightly reduced through averaging. Thus, the RPM model (see

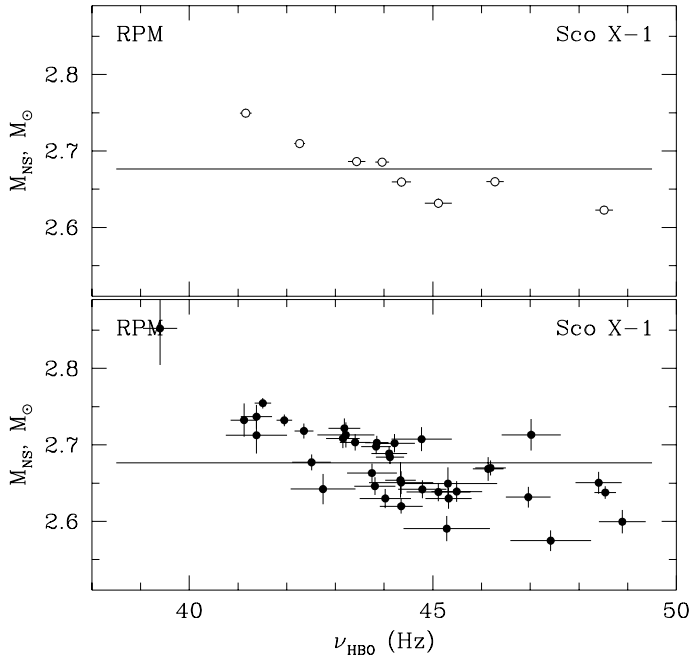

Fig. 7. NS mass versus observed HBO frequency ν_{HBO}. The solid line indicates a constant fit to the data. The lower panel shows individual observations of Scorpius X-1 with a duration up to ~ 3.5 ks. The upper panel shows the same observations as in the lower panel averaged over five points according to the frequency ν_{HBO}.

Table 4) is inconsistent ($r_s = -1$; the total negative correlation between M_{NS} and $\bar{\nu}_{HBO}$) and the assumed NS mass is not an invariant in this model.

Allowance for the second harmonic in determining the low-frequency QPO peak (more specifically, $\bar{\nu}_{HBO} = 1/2(\nu_{HBO} + 1/2\nu_{2HBO})$) results in a reduction of the correlation coefficient r_s for δ in the TLM, while the reverse is true for M_{NS}. In particular, we see from Fig. 8 that the data points are well fitted by a straight line: $\chi^2_{red} = 4.31$ (see Table 2, where $\chi^2_{red} = 16.3$ for the same case but for a constant fit to the data). Figures 6 and 8 (upper panels) show that averaging can reduce the stochastic scatter when determining the model invariants. However, for the TLM (see Fig. 6), δ is virtually constant, $\bar{\delta} = 5.55$, with the rms deviation $\sigma_{\bar{\delta}} = 0.03$ (which is $\approx 0.5\%$), while for the RPM (see Fig. 8), M_{NS} strongly correlates with $\bar{\nu}_{HBO}$ and is incompatible with a constant (the rms deviation is $\sigma_{\bar{M}_{NS}} \approx 1.7\%$, which roughly corresponds to $\sigma_{M_{NS}}$; see Table 2).

5. DISCUSSION AND RESULTS

Both theoretical models suggest the existence of invariants. These invariants are the tilt of the magnetosphere to the disk normal δ for the TLM and the NS mass M_{NS} and its relative angular momentum a for the RPM in the Kerr approximation. Since the RPM did not consider the quadrupole moment of the compact source and disregarded its oblateness (which can give a contribution of $\sim 10 - 15\%$ to the nodal precession frequency), we managed to avoid the inclusion of various theoretical equations of state for neutron stars in our analysis. However, it was of interest to

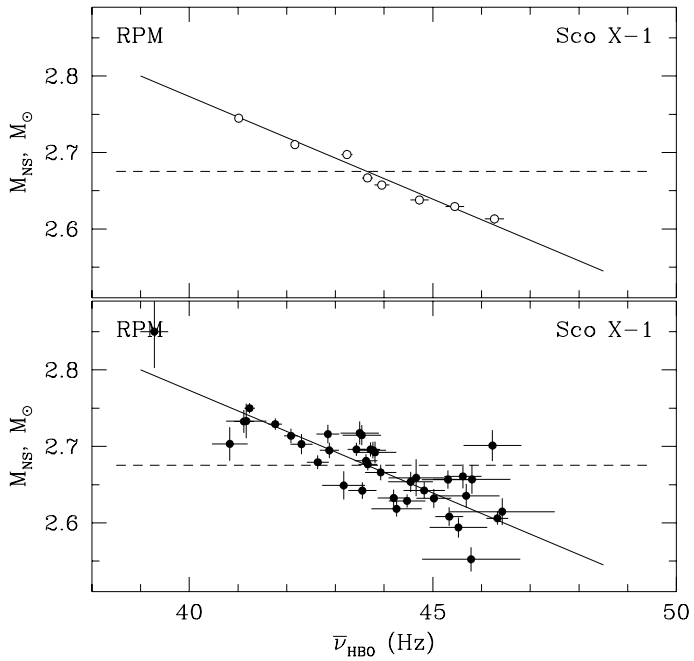

Fig. 8. NS mass versus observed HBO frequency $\nu_{nod} \equiv \bar{\nu}_{mHBO} = 1/2(\nu_{HBO} + 1/2\nu_{2HBO})$. The solid line indicates a constant fit to the data. The lower panel shows individual observations of Scorpius X-1 with a duration up to ~ 3.5 ks. The upper panel shows the same observations as in the lower panel averaged over five points according to the frequency ν_{HBO}.

compare our results with the constraints imposed on the equations of state. Figure 9 shows some of these constraints taken from Miller et al. (1998). The curves correspond to the mass–radius relation for nonrotating neutron stars. Although the angular velocity for Scorpius X-1 is nonzero, the correction for spin (here, $\nu_s \approx 200 - 400$ Hz) can be disregarded.

The assumed NS mass M_{NS} and the Keplerian orbital radius R of the particle rotating around it (see Fig. 9) derived from Eqs. (7)–(9) must be consistent with the constraints imposed by the equations of state. More specifically, $M_{NS} < M_{EOS}$, $R > R_{EOS}$ (here, M_{EOS} and R_{EOS} are the NS mass and radius for various equations of state). Only the equation of state "L" suggest that a massive NS (in our case, $\sim 2.7 M_\odot$) could exist and it agrees with the derived M_{NS} in the two cases ($\nu_{nod} = \nu_{HBO}$ and $2\nu_{nod} = \nu_{HBO}$). At the same time, the other two equations of state ("A" and "UU") are incompatible with the RPM results in the Kerr (i.e., with NS rotation) approximation. Moreover, we obtained M_{NS} for Cygnus X-2 that was compatible, within the error limits ($M_{NS} = 2.69 \pm 0.10$ for $\nu_{nod} = \nu_{HBO}$ and $M_{NS} = 2.29 \pm 0.09$ for $2\nu_{nod} = \nu_{HBO}$; Kuznetsov 2002), with M_{NS} for Scorpius X-1 (see Table 2). Such a coincidence is not an argument for the relativistic precession model either.

In addition, we showed that a nonparametric test for correlation between the assumed NS mass in the RPM and the HBO frequency yields a positive result. Thus, the RPM is not a self-consistent model in which the invariants are conserved and the derived mass of the compact object is large enough for the existing equations of state for neutron stars. At the same time, for the transition-

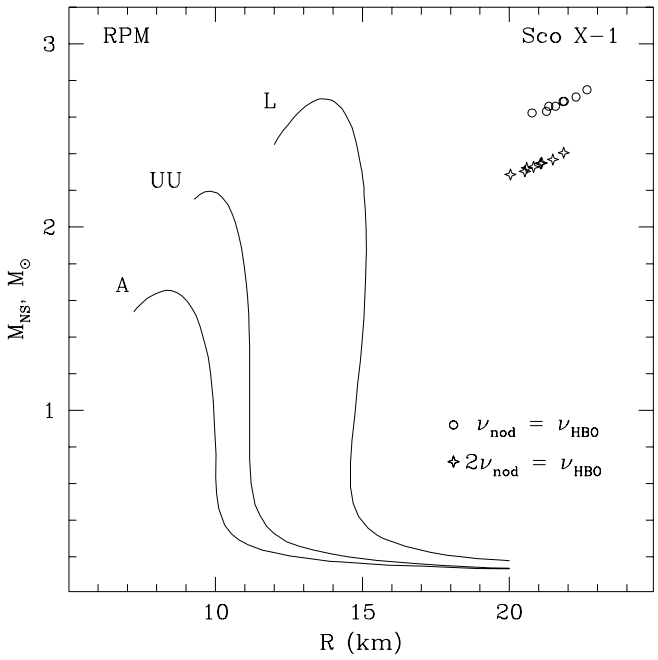

Fig. 9. Relationship of the NS mass to the nodal precession frequency and Keplerian orbital radius. The circles correspond to the mass–radius relation in the case where the nodal precession frequency is identically equal to the HBO frequency ν_{HBO}; the diamonds correspond to the case where it is assumed to be its even harmonic (for more details, see the text). The solid lines [taken from Miller et al. (1998)] represent the mass-radius relations for several equations of state for neutron stars.

layer model, the derived value is compatible with a constant under certain conditions (e.g., using the theory of nonlinear oscillations; for more details, see Kuznetsov and Titarchuk 2002). If the uncertainty in the calculated angle δ does not exceed $\sim 2\%$ (which is lower than the rms deviation for δ in Scorpius X-1; see Table 1), then its value may be assumed to be constant.

The observed inconsistency of the RPM may stem from the fact that the orbital inclination of the test particle in the model simplification is assumed to be infinitesimal. An exact solution for an arbitrary inclination is given in Sibgatullin (2001). In such an analysis, the frequency ν_{HBO} for fixed mass and angular momentum can change by a factor of ~ 3 as the inclination changes from 0 to $\pi/2$ (for the marginally stable orbit at $M_{NS} = 2M_\odot$ and $\nu_\phi = 1200$ Hz). This dispenses with the need to take the nodal precession frequency ν_{nod} to be equal to 1/2 of ν_{HBO} to obtain more acceptable NS-star masses.

In addition, it is worth noting that the angle δ in the RPM may not be strictly an invariant. Higher energy release in the disk can affect the curvature of its inner region. The tilt angle δ between the magnetospheric axis and the normal to the disk surface can then differ for different source fluxes. As a result, the angles δ can differ for the same ν_{HBO} (see Figs. 5 and 6).

Tabl. 3. Correlation between model invariants, δ in the TLM and M_{NS} in the RPM, and HBO frequency.

Parameter	Model			
	TLM		RPM	
	$\nu_L = \nu_{HBO}$	$\nu_L = \bar{\nu}_{HBO}{}^a$	$\nu_{nod} = \nu_{HBO}$	$\nu_{nod} = \bar{\nu}_{HBO}{}^a$
r_s	0.567	0.359	–0.715	–0.789
Prob	2×10^{-4}	3×10^{-2}	3×10^{-7}	2×10^{-9}
N, bin	39	39	39	39

$^a\bar{\nu}_{HBO} = 1/2(\nu_{HBO} + 1/2\nu_{2HBO})$

Note. We used the individual observations shown in the lower panels of Figs. 5-8. The Spearman coefficient r_s close to 1 or -1 corresponds to a total positive or negative correlation between the two quantities. The probability that the observed correlation is the result of purely statistical fluctuations is given for each case.

Tabl. 4. Correlation between model invariants, δ in the TLM and M_{NS} in the RPM, and HBO frequency.

Parameter	Model			
	TLM		RPM	
	$\nu_L = \nu_{HBO}$	$\nu_L = \bar{\nu}_{HBO}{}^a$	$\nu_{nod} = \nu_{HBO}$	$\nu_{nod} = \bar{\nu}^a_{HBO}$
r_s	0.738	0.595	–0.929	–1.000
Prob	3.7×10^{-2}	1.2×10^{-1}	8.6×10^{-4}	0.0
N, bin	8	8	8	8

$^a\bar{\nu}_{HBO} = 1/2(\nu_{HBO} + 1/2\nu_{2HBO})$

Note. We used the data (averaged over four or five observations) shown in the upper panels of Figs. 5-8. The Spearman coefficient r_s close to 1 or -1 corresponds to a total positive or negative correlation between the two quantities. The probability that the observed correlation is the result of purely statistical fluctuations is given for each case.

ACKNOWLEDGMENTS

This study was supported in part by the Program of the Russian Academy of Sciences "Astronomy: Nonstationary Astronomical Phenomena", the Russian Foundation for Basic Research (project no. 02-02-17347), and grant no. 00-15-99297 of the President of Russia. I used the RXTE data retrieved from the Goddard Space Flight Center Electronic Archive. I wish to thank L. Titarchuk, B. Stone, N. White, J. Swank, Ph. Newman, and J. Repaci for the opportunity to work with the RXTE archival data on CR-ROMs. I am grateful to the referee for helpful remarks and comments.

REFERENCES

J. M. Berdeen, W. H. Press, and S. A. Teukolski, Astrophys. J. **178**, 374 (1972).

H. Bradt, R. Rotschild, and J. Swank, Astron. Astrophys., Suppl. Ser. **97**, 335 (1993).

G. Hasinger and M. van der Klis, Astron. Astrophys. **225**, 79 (1989).

K. Jahoda, J. Swank, A. Giles, *et al.*, *EUV, X-ray and Gamma-ray Instrumentation for Astronomy VII,* Ed. by O. Siegmund and M. Gummin, Proc. SPIE **2808**, 59 (1996).

S. Kato, Publ. Astron. Soc. Jpn. **42**, 99 (1990).

S. I. Kuznetsov, Pis'ma Astron. Zh. **27**, 919 (2001) [Astron. Lett. **27**, 790 (2001)].

S. I. Kuznetsov, Pis'ma Astron. Zh. **28**, 88 (2002) [Astron. Lett. **28**, 73 (2002)].

S. Kuznetsov and L. Titarchuk, Astrophys. J. **571**, 137L (2002).

L. D. Landau and E. M. Lifshitz, *Course of Theoretical Physics,* Vol. 1: *Mechanics* (Nauka, Moscow, 1965; Pergamon, New York, 1988).

M. C. Miller, F. K. Lamb, and D. Psaltis, Astrophys. J. **508**, 791 (1998).

S. Morsink and L. Stella, Astrophys. J. **513**, 827 (1999).

T. Okazaki, S. Kato, and J. Fukue, Publ. Astron. Soc. Jpn. **39**, 457 (1987).

V. Osherivich and L. Titarchuk, Astrophys. J. **522**, 113 (1999).

V. Osherovich, I. Tzur, and E. Gliner, Astrophys. J. **284**, 412 (1984).

N. R. Sibgatullin, Pis'ma Astron. Zh. **27**, 929 (2001) [Astron. Lett. **27**, 799 (2001)].

L. Stella, M. Vietry, and S. M. Morsink, Astrophys. J. **524**, L66 (1999).

L. Titarchuk, V. Osherivich, and S. Kuznetsov, Astrophys. J. **525**, L129 (1999).

M. van der Klis, *Timing Neutron Stars,* Ed. by H. Ögelman and E. P. J. van der Heuvel (Kluwer, Dordrecht, 1989), NATO ASI Ser., Ser. C, Vol. 262, p. 27.

M. van der Klis, Annu. Rev. Astron. Astrophys. **38**, 717 (2000).

M. van der Klis, J. H. Swank, W. Zhang, *et al.*, Astrophys. J. **469**, L1 (1996).

M. van der Klis, R. Wijnands, K. Horne, and W. Chen, Astrophys. J. **481**, L97 (1997).

A. Vikhlinin, E. Churazov, and M. Gilfanov, Astron. Astrophys. **287**, 73 (1994).

Translated by V. Astakhov